Journal of Photochemistry and Photobiology A: Chemistry 206 (2009) 155–163

Contents lists available at ScienceDirect

Journal of Photochemistry and Photobiology A: Chemistry

journal homepage: www.elsevier.com/locate/jphotochem

Meta-substituted Ru^{II} rigid rods for sensitization of TiO_2

Maria Abrahamsson[a], Olena Taratula[c], Petter Persson[d,*], Elena Galoppini[c,*], Gerald J. Meyer[b,**]

[a] Department of Chemistry, Johns Hopkins University, 3400 N Charles Street, Baltimore, MD 21218, United States
[b] Department of Chemistry and Department of Materials Science and Engineering, Johns Hopkins University, 3400 N Charles Street, Baltimore, MD 21218, United States
[c] Chemistry Department, Rutgers University, 73 Warren Street, Newark, NJ 07102, United States
[d] Department of Chemical Physics, Lund University, Box 124, SE-221 00 Lund, Sweden

ARTICLE INFO

Article history:
Received 15 January 2009
Received in revised form 11 June 2009
Accepted 14 June 2009
Available online 24 June 2009

Keywords:
Ru compounds
MLCT excited states
Titanium dioxide
DFT calculations
Meta-substitution

ABSTRACT

Ruthenium polypyridyl rigid-rod compounds with phenylene–ethynelene (OPE) spacers and an isophthalic acid (Ipa) binding group were synthesized and characterized for sensitization of nanocrystalline TiO_2 (anatase) thin films. Density functional theory predicted that the most stable structure oriented the isophthalic group about 45° from normal to the TiO_2 surface. Comparative experimental studies of *meta*- and *para*-isomers revealed small changes in the ground state absorption spectra and very similar excited state and redox properties. The excited state injection yields ($\phi_{inj} = 0.15 \pm 0.03$) into nanocrystalline TiO_2 and the subsequent charge recombination rates were found to be insensitive to the isomer utilized. Meta-substitution enabled the synthesis of sensitizers with two Ru^{II} sensitizers that displayed enhanced sunlight absorption relative to the monomeric compound.

1. Introduction

There is continued interest in $Ru(bpy)_3^{2+}$ and its many derivatives for applications in dye-sensitized solar cells, artificial photosynthesis, and sensors and switches [1–6]. For these applications, Ru^{II} compounds are often anchored to conductive substrates. With metal oxide substrates, this is usually accomplished by surface reactions with COOH or $P(O)(OH)_2$ functional groups introduced onto the $Ru(bpy)_3^{2+}$ complex. These functionalities can be incorporated directly onto the pyridine rings of bipyridine or at the end of a molecular bridge motif that acts as a spacer between the Ru^{II}-center and the substrate. For solar cell applications molecular spacers allow the electronic coupling between the sensitizer and the semiconductor to be controlled such that the ratio of the rate constants for charge injection and charge recombination can be optimized. With molecular spacers both the structure of the bridge and the number of anchoring units can be varied. Systematic studies of such materials have already provided fundamental insights into the factors that control excited state relaxation and interfacial electron transfer [1,7–12].

Rod-like bridges, especially those comprised of oligophenylene–ethynylene (OPE) bridges that terminate with carboxylic acid anchoring groups, have been investigated by us and others to study how the bridge affects interfacial electron transfer processes [8–19]. In particular, an OPE bridge with an isophthalic (Ipa) anchoring motif with two COOH groups has been employed for the sensitization of anatase TiO_2 nanocrystallites. For example, pyrene terminated rigid rods quantitatively injected electrons into TiO_2 upon laser excitation [20]. The pyrene extinction coefficient and absorption spectrum were found to be dependent on the number of phenylene–ethynylene units in the bridge [14]. Similarly, Ru^{II}-terminated rigid rods also showed rapid and efficient excited state electron injection into TiO_2.

In all previous work with Ru^{II}-rigid rod sensitized TiO_2, the ethynylene units were substituted in the *para*-positions of the phenyl rings. Herein, we report photophysical studies of Ru^{II}-rigid rods with *meta*-substitution, Scheme 1 and their behavior on mesoporous nanocrystalline TiO_2 thin films. A possible advantage of *meta*-substitution versus *para*-substitution for the Ru^{II}-rigid rod compounds reported here is that the former allows multiple chromophores to be linked to the same anchoring unit. Here we have explored the behavior with two Ru^{II} chromophoric units that enhance the solar light harvesting, but other chromophores can be imagined as well. Our work was also motivated by previous studies of donor-bridge-acceptor compounds with *para*- and *meta*-conjugated phenyl acetylene bridges [21–23]; charge separation times were similar for the two isomers but recombination was a factor of 10 times slower for the meta conjugated bridge [21]. Here it was of interest to examine whether similar behavior would be observed with the Ru^{II}-rigid rods in fluid solution and at sensitized TiO_2 interfaces. Computational modelling is becoming

* Corresponding authors.
** Corresponding author at: Department of Chemistry, Johns Hopkins University, 3400 N. Charles Street, Baltimore, MD 21218, United States. Tel.: +1 410 516 7319; fax: +1 410 516 7044.
E-mail addresses: petter.persson@chemphys.lu.se (P. Persson), galoppin@andromeda.rutgers.edu (E. Galoppini), meyer@jhu.edu (G.J. Meyer).

1010-6030/$ – see front matter © 2009 Elsevier B.V. All rights reserved.
doi:10.1016/j.jphotochem.2009.06.002

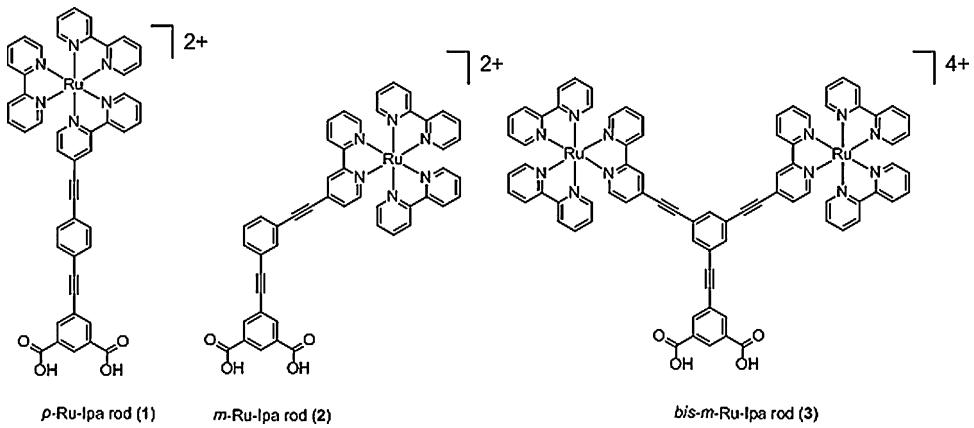

Scheme 1. The *para*- and *meta*-Ru^{II} rigid rod isomers (*p*-Ru-Ipa rod and *m*-Ru-Ipa rod) and the bimetallic compound (*bis-m*-Ru-Ipa rod) investigated in this work. The anions were PF_6^- ions in all cases.

a useful tool to complement experimental work on dye-sensitized semiconductors [24–29], and was used here for this reason and to predict the optimal rigid rod structure of these increasingly complex sensitizer–semiconductor interfaces.

2. Experimental

2.1. Synthesis

2.1.1. General

^1H NMR (499.90 MHz) and ^{13}C (124.98 MHz) spectra were recorded on a Varian INOVA 500 spectrometer. The ^1H and ^{13}C NMR chemical shifts δ are given in ppm and were referenced to tetramethylsilane or to the central line of the solvent. NMR spectra were recorded at room temperature in deuterated chloroform or dimethyl sulfoxide as indicated. Coupling constants (J) are reported in Hz. High resolution mass spectra (HRMS) were obtained at a commercial facility (MSU Mass Spectrometry Facility). Column chromatography was performed using silica gel from Sorbent Technologies standard grade (32–63 μm particle size). TLC was performed on Sorbent Technologies silica gel plates using UV light as the developing agent. THF was purchased anhydrous (Fisher) and then distilled under nitrogen atmosphere from sodium benzophenone ketyl. Triethylamine were purchased from Fisher and freshly distilled from CaH_2 under nitrogen. Other organic reagents, including Pd catalysts for Sonogashira cross-coupling, and solvents were used as purchased from Aldrich or Fisher.

2.1.2. Procedures

The synthesis of *p*-Ru-Ipa-rod (**1**) has been published [11]. Ru^{II}-polypyridyl-based *m*-conjugated rigid-rods **2** and **3** were synthesized according to Scheme 2. The synthesis of precursors **4** and **4a** was reported elsewhere [17]. A well-known procedure [30,31] was used to prepare the 4-iodo-2,2′-bipyridine compound **5**. All Sonogashira cross-coupling reactions were performed under inert atmosphere in glassware flamed under vacuum, and using anhydrous solvents. Standard workup procedures involve multiple (∼3) extractions with the indicated organic solvent, followed by washing of the combined organic extracts with water or brine, drying over Na_2SO_4 and removal of solvents *in vacuo*. All yields are reported after purification by column chromatography or crystallization.

2.1.3. Cross-coupling with 4-iodo-2,2′-bipyridine (Step a in Scheme 2)

The mixture of triethylamine/THF (14 mL, 1/1) was added to the flask which was charged with **4** (0.31 mmol, 100.0 mg), 4-iodo-2,2′-bipyridine **5** (0.34 mmol, 96.1 mg), $Pd_2(dba)_3$ (0.034 mmol, 19.6 mg) and P(*o*-tol)$_3$ (0.28 mmol, 85.0 mg). The reaction mixture was stirred under nitrogen at rt for 12 h. The solvent was evaporated in *vacuo*. The crude product was purified by flash chromatography column (silica gel, CH_2Cl_2). The product **6** (0.23 mmol, 110.0 mg, yield: 74%) was obtained as a white solid. ^1H NMR δ_H (500 MHz, $CDCl_3$): 8.71 (1 H, d, J = 5 Hz), 8.69 (1 H, d, J = 5 Hz), 8.65 (1 H, s), 8.56 (1 H, s), 8.42 (1 H, d, J = 8 Hz), 8.38 (2 H, s), 7.84 (1 H, t, J = 8 Hz), 7.77 (1 H, s), 7.57 (1 H, d, J = 8 Hz), 7.56 (1 H, d, J = 8 Hz), 7.41 (1 H, d, J = 5 Hz), 7.40 (1 H, t, J = 8 Hz), 7.35 (1 H, t, J = 5.5 Hz), 3.98 (6 H, s, COOCH_3). ^{13}C NMR δ_C (125 MHz, $CDCl_3$): 165.6 (*C*=*O*), 156.3, 149.3, 137.0, 136.6, 135.5, 134.9, 133.2, 133.0, 132.8, 132.2, 132.1, 131.0, 130.3, 128.8, 125.3, 124.0, 123.2, 123.1, 122.8, 121.2 (C_{Ar}, CH_{Ar}); 92.7, 90.1, 88.2, 87.8 (*C*≡*C*); 52.6 (2 C, COOCH_3). The same procedure was used to react **4a** (100.0 mg, 0.30 mmol) with 4-iodo-2,2′-bipyridine (**5**) (0.68 mmol, 192.0 mg) in the presence of $Pd_2(dba)_3$ (0.068 mmol, 39.2 mg) and P(*o*-tol)$_3$ (0.56 mmol, 170 mg) to obtain **6a** (143.0 mg, 0.22 mmol, yield: 75%, white solid). ^1H NMR δ_H (500 MHz, $CDCl_3$): 8.72 (2 H, d, J = 5 Hz), 8.70 (2 H, d, J = 5 Hz), 8.67 (1 H, s), 8.57 (2 H, s), 8.42 (2 H, d, J = 8 Hz), 8.40 (2 H, s), 7.85 (2 H, t, J = 8 Hz), 7.75 (2 H, s), 7.75 (1 H, s), 7.43 (2 H, d, J = 5 Hz), 7.36 (2 H, t, J = 5.5 Hz), 3.99 (6 H, s, COOCH_3). ^{13}C NMR δ_C (125 MHz, $CDCl_3$): 165.5 (*C*=*O*), 156.4, 155.4, 149.3, 149.3, 137.0, 136.6, 135.1, 135.0, 131.7, 131.0, 130.5, 125.3, 124.1, 123.7, 123.7, 123.4, 123.3, 121.1 (C_{Ar}, CH_{Ar}); 91.6, 89.1, 89.0, 88.6 (*C*≡*C*); 52.6 (2 C, COOCH_3).

2.1.4. Formation of Ru^{II} Compounds (Step b in Scheme 2)

Compound **6** (0.21 mmol, 100.0 mg) was dissolved in the mixture of THF/ethanol (15 mL, 1/2, freeze pump thaw) under inert atmosphere. Slight excess of $Ru(bpy)_2Cl_2{\cdot}2H_2O$ (0.22 mmol, 114.4 mg) was added to the solution and the mixture was refluxed overnight, then cooled to room temperature and filtered. Addition of aqueous $NaPF_6$ (2.8 mmol, 470.4 mg) solution to the filtrate produced a precipitate, which was collected and washed with water to afford the Ru^{II} compound **7** (0.16 mmol, 191.6 mg, yield: 77%) as an orange powder. ^1H NMR δ_H (500 MHz, acetone-d_6): 8.95 (2 H, m), 8.82 (4 H, m), 8.60 (1 H, d, J = 4 Hz), 8.48 (2 H, m), 8.35 (2 H, m), 8.22 (6 H, m), 8.08 (4 H, m), 7.93 (2 H, m), 7.62 (6 H, m), 7.50 (1 H, m), 3.98 (6 H, s, COOCH_3). ^{13}C NMR δ_C (125 MHz, acetone-d_6): 165.7 (*C*=*O*), 158.6, 158.1, 157.9, 157.8, 156.7, 155.4, 153.2, 152.9, 152.7, 152.4, 152.1, 149.8, 137.4, 136.6, 135.8, 135.1, 133.6, 133.4, 132.9, 132.6, 132.5, 131.4, 130.7, 129.2, 125.7, 124.4, 123.6, 123.4, 122.9, 121.8 (C_{Ar}, CH_{Ar}); 93.7, 91.1, 88.8, 87.9 (*C*≡*C*); 53.4 (2 C, COOCH_3). IR-ATR (cm^{-1}): 2916, 2851 (*C*–*H*), 2210 (*C*≡*C*), 1724 (*C*=*O*), 1599 (*C*=C_{Ar}), 1439 (*C*=C_{Ar}), 1332, 1239 (*C*–*O*), 993, 838. Compound **6a** (0.15 mmol, 100 mg) reacted in the same conditions with $Ru(bpy)_2Cl_2{\cdot}2H_2O$ (0.32 mmol, 168.1 mg) to give **7a** (0.12 mmol, 240.6 mg, 76%). ^1H NMR δ_H (500 MHz, acetone-d_6): 8.99 (2 H, m), 8.94 (2 H, m), 8.83 (4

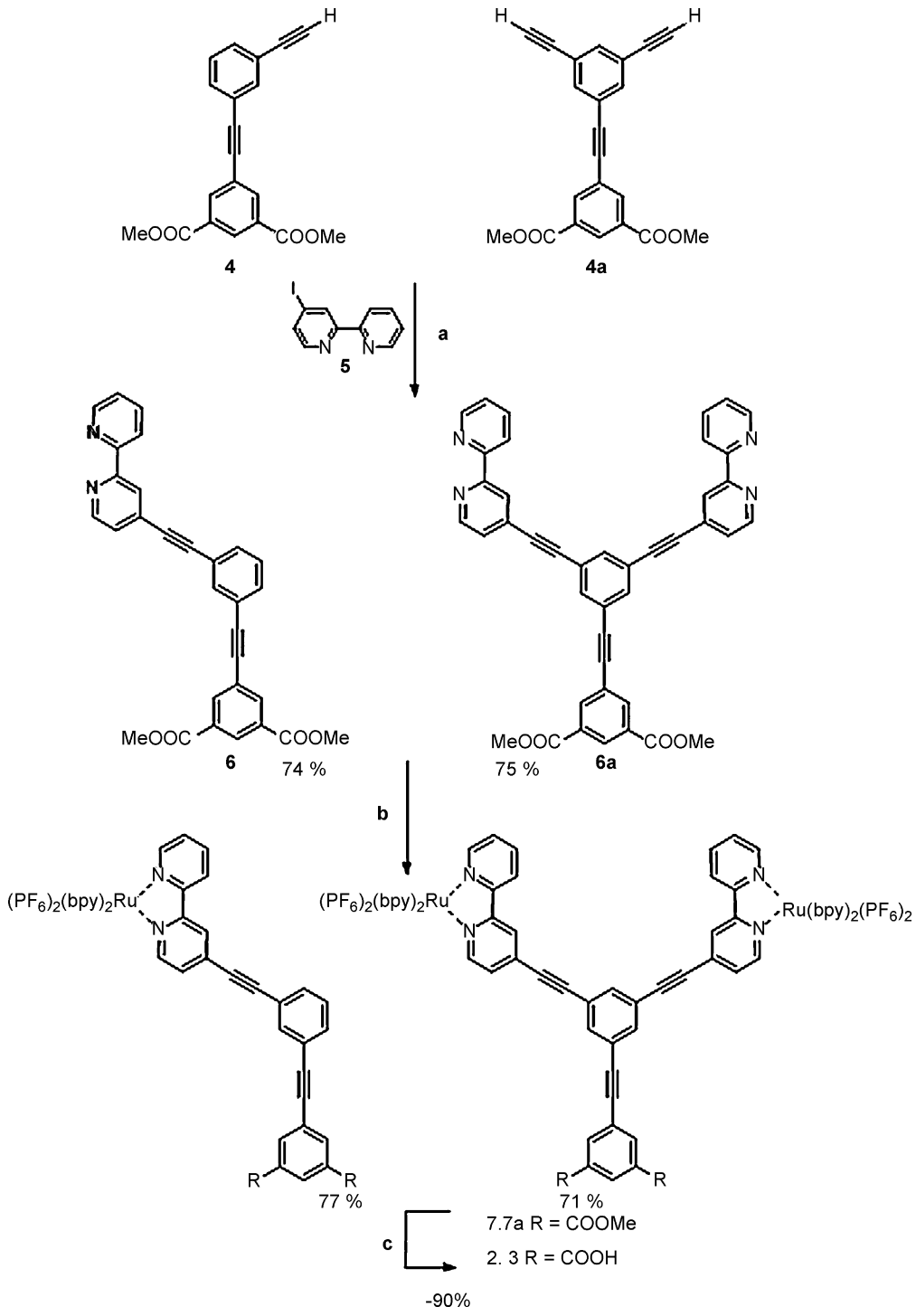

Scheme 2. Reagents and conditions[a] for synthesis of the compounds **2** and **3**. [a]Step a: $Pd_2(dba)_3$, P(*o*-tol)$_3$, THF/Et_3N, rt. Step b: $Ru(bpy)_2Cl_2{\cdot}2H_2O$, $NaPF_6$. Step c: (1) NaOH, H_2O/THF; (2) 10% HCl (aq).

H, m), 8.73 (2 H, m), 8.61 (4 H, m), 8.49 (2 H, m), 8.39 (2 H, m), 8.23 (12 H, m), 8.07 (6 H, m), 7.95 (2 H, m), 7.61 (12 H, m), 7.48 (2 H, m), 3.98 (6 H, s, COOCH_3). ^{13}C NMR δ_C (125 MHz, acetone-d_6): 165.6 (*C*=*O*), 158.7, 158.3, 157.7, 157.6, 156.7, 156.5, 155.6, 153.2, 152.9, 152.7, 152.3, 152.1, 149.7, 149.3, 137.4, 136.8, 135.3, 135.1, 131.8, 131.4, 130.6, 125.7, 124.3, 123.9, 123.8, 123.6, 123.7, 121.4 (C_{Ar}, CH_{Ar}); 93.2, 90.1, 89.6, 88.8 (*C*≡*C*); 53.2 (2 C, $COOCH_3$). IR-ATR (cm^{-1}): 2931, 2850 (*C*–*H*), 2216 (*C*≡*C*), 1725 (*C*=*O*), 1602 (*C*=C_{Ar}), 1445 (*C*=C_{Ar}), 1332, 1248 (*C*–*O*), 836. HRMS-FAB calcd. for $C_{82}H_{58}O_4N_{12}Ru_2P_3F_{18}$ (M^+-PF_6): 1913.1750. Found: 1913.1740.

2.1.5. Hydrolysis (Step c in Scheme 2)

The ester **7** (30.0 mg, 0.025 mmol) was dissolved in acetonitrile (10 mL) and NaOH (40.0 mg, 1.0 mmol) was added to the solution. The reaction mixture was stirred at rt overnight. The basic aqueous layer was extracted with chloroform, then 10% aqueous HCl was added dropwise to approximately pH 2. The precipitate was filtered and rinsed with water to afford **2** as a red powder (26.5 mg, 0.023 mmol, yield: 90%). IR-ATR (cm^{-1}): 3250-2500 (*O*–*H*), 2915, 2848 (*C*–*H*), 2210 (*C*≡*C*), 1707 (*C*=*O*), 1601 (*C*=C_{Ar}), 1439 (*C*=C_{Ar}), 1225 (*C*–*O*), 840. HRMS-FAB calcd. for $C_{48}H_{32}O_4N_6RuPF_6$ (M^+-PF_6):

1003.1180. Found: 1003.1168. The same procedure was used to convert **7a** (40.0 mg, 0.02 mmol) into **3** (36.0 mg, 0.018 mmol, yield: 91%). IR-ATR (cm^{-1}): 3250–2500 (*O–H*), 2920, 2845 (*C–H*), 2210 (*C≡C*), 1713 (*C=O*), 1602 (*C=C*$_{Ar}$), 1437 (*C=C*$_{Ar}$), 1230 (*C–O*), 837.

2.2. Electrochemistry

Cyclic voltammetry was performed with a BAS potentiostat under an atmosphere of nitrogen at room temperature with a conventional three-electrode configuration. A glassy carbon electrode (2 mm diameter) was used as the working electrode along with a platinum wire auxiliary electrode and a Ag/AgCl reference electrode in 0.1 M $TBAClO_4/CH_3CN$ electrolyte. The potential of the Ag/AgCl electrode was measured against ferrocene and converted to the NHE scale. Redox potentials ($E_{1/2}$) were determined from the average of anodic and cathodic peak potentials at scan rates of 100 mV/s. Differential pulse voltammetry experiments were carried out at room temperature under nitrogen atmosphere and monitored at a scan rate of 20 mV/s, with pulse amplitude 50 mV, and pulse period 200 ms.

2.3. Preparation of semiconductor thin films

Transparent and mesoporous thin films of nanocrystalline TiO_2 were prepared according to procedures previously described [32]. The semiconductor films were pretreated with KOH at pH 11 and rinsed with acetonitrile prior to immersion in mM CH_3CN solutions of the Ru-rods. The adsorption reactions were typically carried out over-night. Sensitized films were thoroughly rinsed with CH_3CN before experiments were performed.

2.4. Spectroscopy

Ground state UV–vis absorbance measurements were performed on a Hewlett-Packard 8453 diode array spectrophotometer or on a Varian Cary 50 UV-Vis spectrophotometer. Nanosecond transient absorption measurements were performed with a flash-photolysis setup, with a pulsed Xe-lamp (150 W) as probe light source, a Nd:YAG (Brilliant B) laser was used for production of excitation light, either 532 nm from frequency doubling of the fundamental 1064 nm line, or 417 nm produced from Raman-shifting of the frequency tripled output at 355 nm, fwhm of the laser pulse ca. 8 ns, with a 1 Hz repetition rate, described in detail elsewhere [33]. Time-resolved photoluminescence, PL, decays were measured after excitation with a nitrogen laser (PTI) pumping a dye laser. Steady state PL spectra were recorded in a Spex Fluorolog II and corrected for spectral sensitivity. All samples were deoxygenated with either N_2 or Ar for at least 15 min prior to measurements. Sensitized films were placed diagonally in 1 cm × 1 cm cuvettes with acetonitrile or $LiClO_4$-containing acetonitrile as solvent. Unsensitized films were used as references for UV–vis absorption spectra. The 77 K measurements were performed in MeOH:EtOH 1:4 (v/v) mixture, and samples were cooled down to 77 K with liquid nitrogen in a cold finger Dewar setup.

2.5. Computational methods

Full Density Functional Theory (DFT) quantum chemical geometry optimizations have been carried out for the Ipa anchor group binding to a $(TiO_2)_{46}$ cluster which belongs to a set of model nanocrystals that we have developed for such purposes [34–36]. The calculations used the B3LYP hybrid functional [37] together with a Valence Double-Zeta (VDZ) basis set that we have previously employed successfully to study the adsorption of other molecules and anchor groups to metal oxide surfaces [34,38]. The calculations were done using the Gaussian03 program [39].

3. Results and discussion

3.1. Electronic absorption spectroscopy and electrochemistry

The UV–vis absorption spectra of the rigid rods in acetonitrile solution are shown in Fig. 1, and electronic absorption and electrochemical properties are summarized in Table 1. All compounds displayed strong transitions in the UV-region, attributed to bipyridine (∼300 nm) and bridge-centered transitions. The expected metal-to-ligand-charge-transfer (MLCT) absorption band was present in the visible region with maximum intensity around 465 nm, which was somewhat red-shifted compared to $Ru(bpy)_3^{2+}$ in solution (MLCT max at 450 nm) [2]. The *p*-Ru-Ipa-rod displayed an additional absorption band around 340 nm assigned to π–π* transitions of the extended OPE motif [17,40]. For rods bound to TiO_2 the higher energy bands were obscured by the absorption of the semiconductor.

As expected the extinction coefficient determined for the bis-*m*-Ru-Ipa-rod was roughly double that of the *m*-Ru-Ipa-rod. More interesting was the fact that the *p*-Ru-Ipa-rod also displayed extinction coefficients that were almost twice those of the *m*-Ru-Ipa-rod. The enhanced extinction coefficient is attributed to the excited electron being delocalized over a larger π-system in the *p*-Ru-Ipa-rod, while the meta-connection induces a break in the conjugation and thus a smaller extinction coefficient. Earlier studies on rigid rods with pyrene as the chromophoric unit also displayed enhanced extinction coefficients for compounds with the bridge connected to the chromophore in the para-position. For rods terminated with pyrene in the meta-position a blue shifted absorption spectra was observed, which is in contrast to the results for the rigid rods in this study [17]. This difference can probably be attributed to a more pronounced symmetry effect upon attachment of the linker motif to pyrene compared to $Ru(bpy)_3^{2+}$ as discussed in reference [17].

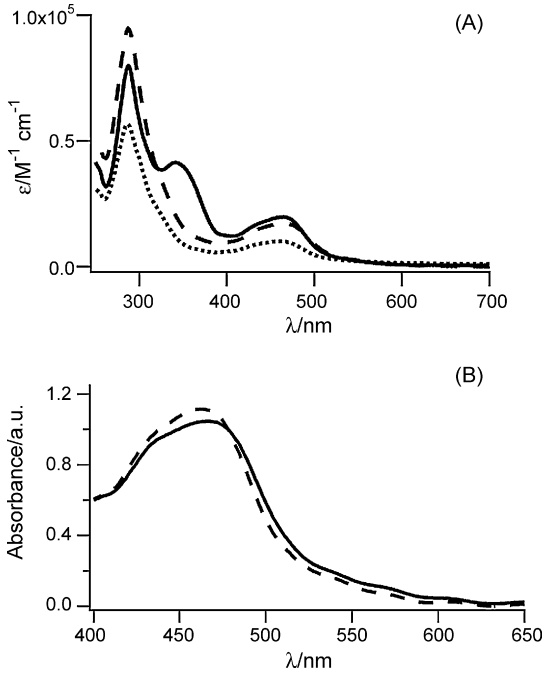

Fig. 1. (A) Absorption spectra of *p*-Ru-Ipa-rod (solid line), *m*-Ru-Ipa-rod (dotted line), and bis-*m*-Ru-Ipa-rod (dashed line) in acetonitrile. (B) The absorption spectra of *m*-bis-Ru-rod/TiO_2 in neat CH_3CN (solid line) and in 0.3 M $LiClO_4/CH_3CN$ (dashed line).

Table 1
Electronic absorption and electrochemical properties of the indicated Ru-rods.[a].

Compound	Absorption λ_{max}, nm ($\varepsilon \times 10^{-4}$ M^{-1} cm^{-1})	$E_{1/2}$ $Ru^{III/II}$, V vs. NHE	ΔG^* (eV)[a]	$E^*_{1/2}$ $Ru^{III/II*}$, V vs. NHE
p-Ru-rod (**1**)	288 (8.0), 341 (4.1), 465 (2.0)	1.54	2.13	−0.59
m-Ru-rod (**2**)	288 (5.6), 468 (1.0)	1.53	2.15	−0.62
bis- *m*-Ru-rod (**3**)	288 (9.4), 465 (1.7)	1.47	2.12	−0.65
p-Ru-rod/TiO_2	350-400 (shoulder), 467	1.50	2.13[b]	−0.63
m-Ru-rod//TiO_2	465	1.53	2.15[b]	−0.62
bis-*m*-Ru-Ipa-rod/TiO_2	467	1.49	2.12[b]	−0.63

[a] All measurements made at room temperature in CH_3CN or 0.1 M $TBACLO_4/CH_3CN$ (electrochemistry) except for the Gibbs free energy stored in the excited state, ΔG^*, which was abstracted from PL spectra data acquired at 77 K in a 4:1 ethanol:methanol glass.

[b] It was assumed that the free energy stored in the excited state remained unchanged upon attachment to TiO_2.

The MLCT absorption spectra remained essentially unchanged in the visible region when the molecules were attached to TiO_2 semiconductor films and immersed in neat acetonitrile. When Li^+ was present in the external acetonitrile solution, a slight increase and a small blue-shift in the absorption spectra were observed. Such data is shown for *m*-Ru-Ipa-rod/TiO_2 in Fig. 1B and was observed for the bis-*m*-Ru-Ipa-rod/TiO_2 and *p*-Ru-Ipa-rod/TiO_2 material as well. Lithium cations are potential-determining ions that are often utilized in dye sensitized solar cells to increase the excited state electron injection yield. Many Ru^{II}-sensitizers with the dcb ligand, where dcb is 4,4′-$(CO_2H)_2$-bpy, display significant red shifts in their visible absorption spectra upon exposure to Li^+ cations [41,42]. Interestingly, with tripodal Ru^{II} sensitizers anchored to TiO_2, where conjugation is disrupted by one or more sp^3 hybridized carbon centers, the MLCT absorption is insensitive to the ionic strength of the acetonitrile solution [42]. The small but significant shifts reported here may therefore reflect continuous conjugation from the carboxylic acid anchoring groups to the Ru(bpy)$_3$-units through the rigid rods.

Cyclic and differential pulse volammetry measurements in fluid acetonitrile electrolyte revealed an oxidation at ∼+1.5 V versus NHE, that was assigned to the $Ru^{III/II}$ redox process, Table 1 [11]. The redox process was best described as quasi-reversible as the anodic and cathodic currents were approximately the same but the peak-to-peak separation measured by cyclic voltammetry was greater than 60 mV. A single $Ru^{III/II}$ wave was observed for the bimetallic rigid-rod compound, indicating that the two metal centers were decoupled in the ground state. Upon attachment to TiO_2, quasi-reversible redox chemistry was also observed and the $Ru^{III/II}$ redox potentials remained essentially unchanged from their values in fluid electrolyte, Table 1. Spectroelectrochemical measurements of the oxidized forms of the rigid-rod compounds anchored to TiO_2 (data not shown) revealed that the Ru^{III} forms showed no significant absorption in the visible region.

Thermochemical cycles were used to estimate the excited state reduction potential, $E_{1/2}$ ($Ru^{III/II*}$), with the experimentally measured ground state reduction potentials, $E_{1/2}(Ru^{III/II})$, and the free energy stored in the thermally equilibrated excited state free energy ΔG^*, Eq. (1):

$$E^*_{1/2}(Ru^{III/II*}) = E_{1/2}(Ru^{III/II}) - \Delta G^* \quad (1)$$

The ΔG^* values were estimated with a tangent line drawn on the high energy side of the corrected photoluminescence spectra at 77 K in a 4:1 ethanol:methanol glass as described further below. It was assumed that the ΔG^* remained unchanged upon attachment of the rigid rods to TiO_2. Ground and excited state reduction potentials are given in Table 1.

3.2. Quantum chemical calculations

Full quantum chemical (B3LYP/VDZ) geometry optimizations were carried out for binding modes involving one or both of the carboxylate anchor groups, with the resulting interfacial structures shown in Fig. 2. Adsorption energies were calculated from differences in total energies between on the one hand the separate cluster and adsorbate and on the other hand the combined system as $E_{ads} = E[(TiO_2)_{46}] + E[Ipa] - E[Ipa\text{-}(TiO_2)_{46}]$. A positive value thus indicates stable adsorption. The single- and double-anchor binding modes were calculated to have adsorption energies of 51 and 85 kcal/mol, respectively. The single anchor value was in reasonable agreement with the published adsorption energy of 42 kcal/mol for isonicotinic acid, which is a pyridine with a carboxylic group in the para-position [34]. The 9 kcal/mol difference in adsorption energy is likely to be partly due the increased acidity of the carboxylic group in Ipa relative to isonicotinic acid ($pKa_1 = 3.70$, $pKa_2 = 4.60$ for Ipa and pKa = 4.90 for isonicotinic acid). The optimized single-anchor geometry suggests that the functionalization of the Ipa unit with a

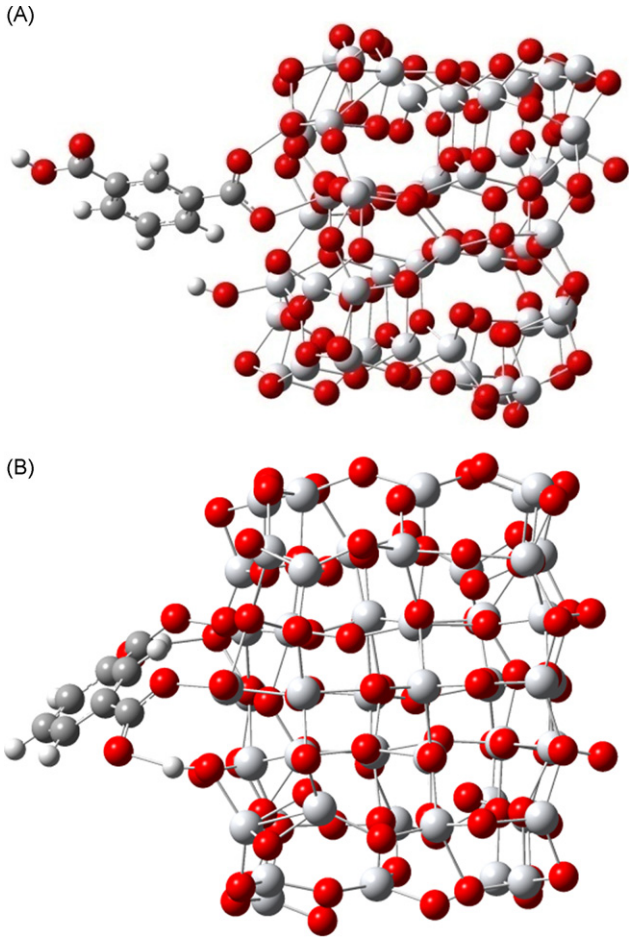

Fig. 2. DFT optimized geometries for (A) single-carboxylate and (B) double-carboxylate binding to a model TiO_2 nanoparticle.

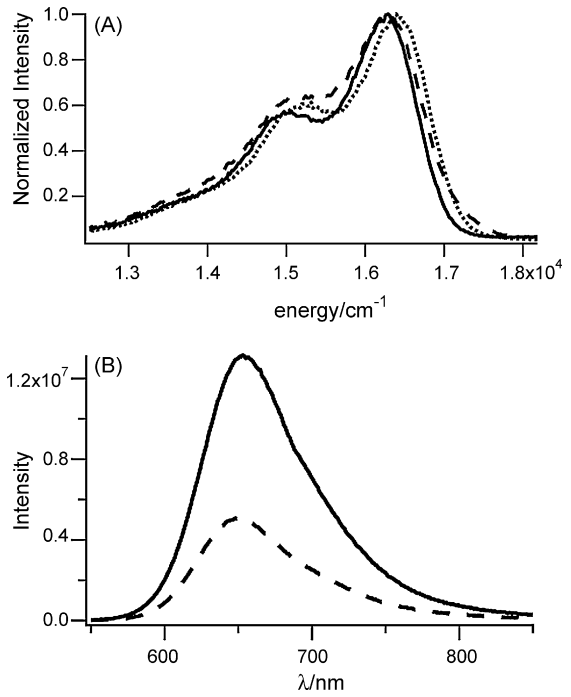

Fig. 3. (A) Steady state photoluminescence, PL, spectra of *p*-Ru-Ipa-rod (solid line), *m*-Ru-Ipa-rod (dotted line), and bis-*m*-Ru-Ipa-rod (dashed line) at 77 K in MeOH:EtOH glass. (B) Photoluminescence spectra of *p*-Ru-Ipa-rod/TiO_2 in neat de-aerated CH_3CN (solid line) and the same *p*-Ru-Ipa-rod/TiO_2 film immersed in 0.3 M $LiClO_4$ CH_3CN solution.

chromophore, possibly linked via a rigid spacer, would result in a structure in which the chromophore (or spacer-chromophore) unit protrudes from the Ipa binding unit essentially parallel to the TiO_2 substrate. Low-energy barriers for twisting the compound around the Ph-COO_{ads} bond relative to the substrate are expected (Figs. 3 and 4).

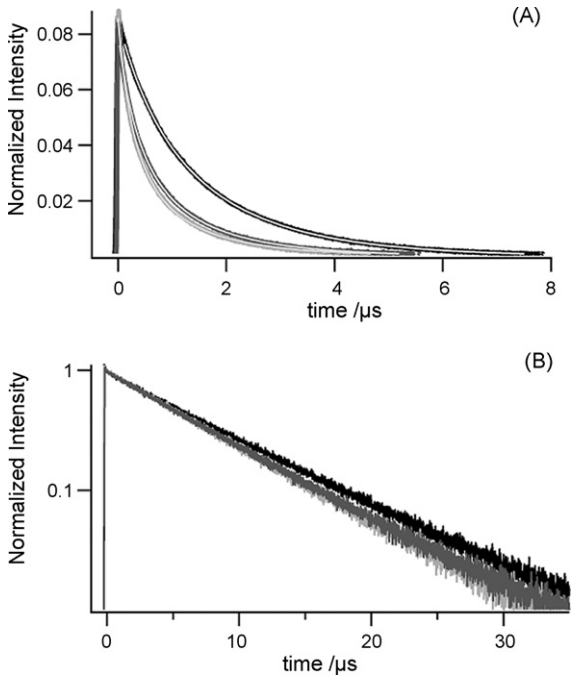

Fig. 4. (A) Time-resolved photoluminescence decays of *p*-Ru-Ipa-rod/TiO_2 (black, upper trace), *m*-Ru-rod-Ipa/TiO_2 (light grey, lower trace) and bis-*m*-Ru-Ipa-rod/TiO_2 (dark grey, middle) in acetonitrile solution. Overlaid are fits to a parallel first- and second-order kinetic model. (B) Time-resolved photoluminescence decays in MeOH:EtOH matrix at 77 K, note the logarithmic *y*-axis. *p*-Ru-Ipa-rod (black), *m*-Ru-Ipa-rod (light grey) and bis-*m*-Ru-Ipa-rod (dark grey).

Interestingly, the double-anchor binding mode was seen to be significantly (34 kcal/mol) more stable than the single-anchor mode. This suggests that the strategy of using Ipa as a more stable binding group for TiO_2-binding compared to a single carboxylate anchor group is worthwhile. This double-anchor adduct energy was, however, significantly less than twice the single-anchor adduct energy which indicates appreciable strain in the formation of the second surface-anchor attachment. By inspection of the resultant double-anchor binding mode, this was ascribed in part to the non-ideal orientation of the two carboxylate groups relative to each other and to the surface, and partly to steric interaction of the phenyl ring with the surface. The optimized geometry obtained in these calculations indicates that the aromatic moiety of the Ipa unit is tilted ca. 45° relative to the surface that would result in a similar tilt in the Ru(bpy) (or spacer-chromophore) unit that may result from unfavourable steric interactions between the para-hydrogen on the Ipa and the semiconductor. Each anchor group is, furthermore, likely to compete for the binding site with other potential adsorbates, such as solvent molecules. The substantial weakening of the second surface-anchor binding therefore means that the overall preferred binding mode may depend on e.g. the chemical environment and the surface coverage.

3.3. Steady state and time resolved photoluminescence

3.3.1. Solution studies

The compounds displayed photoluminescence properties typical of Ru^{II}-polypyridyl ^{3}MLCT states, with the maximum intensity centered around 650 nm, which was slightly red-shifted compared to the parent $Ru(bpy)_3^{2+}$ compound [2]. Photoluminescence quantum yields, quantified by the optically dilute method with $Ru(bpy)_3^{2+}$ as reference, were slightly larger for *m*- and *p*-Ru-Ipa-rods than for the parent $Ru(bpy)_3^{2+}$, while the bimetallic rod displayed a somewhat lower value [2,43]. The excited state lifetimes, as extracted from time-resolved photoluminescence measurements, were in all cases longer than the ~1 μs reported for $Ru(bpy)_3^{2+}$. For *p*- and *m*-Ru-Ipa-rod, this means that both the photoluminescence quantum yield and excited state lifetimes increase, and therefore the radiative and the total non-radiative decay rate constants, calculated according to Eqs. (2a) and (2b), remained at almost the same value as for the reference compound $Ru(bpy)_3^{2+}$.[44] These results suggest that the *m*- and *p*-Ru-Ipa-rod electronic properties were not so different in the excited state. However, for the bimetallic compound, the radiative decay rate was slightly but significantly lower suggestive of an additional non-radiative decay pathway. All compounds exhibited excited states that decayed with single exponential kinetics.

$$k_{rad} = \frac{\Phi}{\tau_{obs}} \quad (2a)$$

$$k_{nr}^{tot} = \frac{1-\Phi}{\tau_{obs}} \quad (2b)$$

At 77 K, the steady state photoluminescence, PL, spectra were centered around 610–615 nm for the three compounds. The spectra displayed vibronic structure, mainly from the 0–0 and 0–1 vibrational transitions. The spectra were very similar in shape but the bis-*m*-Ru-Ipa-rod showed a somewhat broader spectrum and also a smaller ratio between the two vibrational peaks than the monometallic compounds. This suggests a somewhat larger excited state distortion compared to the monometallic *meta*- and *para*-isomers. The time resolved 77 K PL data revealed excited state lifetimes between 6.8 and 7.8 μs, Table 2.

Table 2
Photoluminescence (PL) properties of the compounds in acetonitrile solution (298 K) or in MeOH:EtOH 1:4 (77 K) or on TiO_2 in acetonitrile solution at 298 K, under argon or nitrogen atmosphere.

	CH_3CN and MeOH:EtOH glass							TiO_2 thin film in CH_3CN at 298 K	
	298 K					77 K			
	λ_{max} (nm)	Φ ($\times 10^2$)	τ (μs)	k_{rad} ($\times 10^{-4}$/s^{-1})	k_{nr}^{tot} ($\times 10^{-5}$/s^{-1})	λ_{max} (nm)	τ (μs)	λ_{max} (nm)	k_1 ($\times 10^{-5}$/s^{-1})
p-Ru-rod (**1**)	647	14	2.29	6.1	3.8	614	7.8	655	5.2
m-Ru-rod (**2**)	648	9.5	2.14	4.4	4.2	610	6.8	652	6.5
bis-*m*-Ru-Ipa-rod (**3**)	652	3.3	1.90	1.8	5.0	613	7.0	659	6.2

It has been shown that the radiative rate constant is usually independent of temperature [2], and thus, using the k_{rad} values obtained at room temperature and the excited state lifetimes at 77 K and applying Eqs. (2a) and (2b), the non-radiative decay rate at 77 K can be estimated to be 6.7×10^4 s^{-1} for *p*-Ru-Ipa-rod while the values obtained for the mono- and bimetallic meta isomers were 1.0×10^5 s^{-1} and 1.2×10^5 s^{-1} respectively. The slightly larger non-radiative decay rate in the bimetallic rod reports on non-radiative decay directly to the ground state, and thus is another indication that its excited state is more distorted than that of the *m*- and *p*-Ru-Ipa-rods. In summary the results discussed above points to small differences in the excited state behavior between *m*-Ru-Ipa-rods and *p*-Ru-Ipa-rods while the incorporation of a second chromophore makes a larger difference. Although the non-radiative decay rate is higher in the bimetallic rod, this did not affect the the excited state lifetime to a large extent. This is a significant observation for future design of multichromophoric sensitizers or antenna molecules, since it indicates week electronic communication between the two chromophores. This is also an encouraging result for the more synthetically challenging project to increase light absorption over a broader spectral range through incorporation of two or more different chromophores on the same rod as it indicates unwanted electron and energy transfer reactions may not significantly alter the excited state injection yields.

3.3.2. *MLCT excited states on TiO_2 surfaces*

When attached to TiO_2 thin films and immersed in CH_3CN, the steady state PL spectra of the rigid rods was slightly red-shifted compared to spectra obtained in fluid acetonitrile. The observation of PL reported may seem counter intuitive when considering the rapid femto-second excited state injection that is well documented at Ru^{II} sensitized TiO_2 [1]. However, it should be kept in mind that unless the previously mentioned potential determining ions (H^+ or Li^+) are adsorbed onto the anatase nanocrystallites, the excited state injection yields can be very low [42,45].

Addition of $LiClO_4$ to the solution surrounding the TiO_2 film to a final concentration of 0.3 M indeed resulted in a small but significant blue-shift of the MLCT absorption and the PL spectra of all the rigid rods. This is in contrast to previously reported results for heteroleptic Ru^{II}-sensitizers anchored to TiO_2 through the commonly utilized dcb (4,4′-$(COOH)_2$-2,2′-bipyridine) ligand, where a *red-shift* of the optical spectra were observed when significant concentration of Li^+ were added [41]. The steady state PL intensity was also significantly quenched with Li^+ for *p*-Ru-Ipa-rod/TiO_2 but much less so for *m*-Ru-Ipa-rod/TiO_2. Assuming that the Li^+-induced PL quenching is solely due to excited state electron injection, these data correspond to an increase in the excited state injection yield to 30% for the *p*-Ru-Ipa-rod/TiO_2, 10% for *the m*-Ru-Ipa-rod/TiO_2, and ∼20% for the bis-*m*-Ru-Ipa-rod/TiO_2. Other details of excited state injection are discussed in the following section.

The excited-state decay of the Ru-rigid rods anchored to TiO_2 was non-exponential and was well described by a parallel first- and second-order kinetic model, Equations 3a-b

$$\mathrm{PLI}(t) = B\left(\frac{k_1 \exp(-k_1 t)}{k_1 + p - p\exp(-k_1 t)}\right) \quad (3a)$$

$$p = k_2[\mathrm{Ru}^{2+*}]_{t=0} \quad (3b)$$

where k_1 is a first-order rate constant and equals the sum of the radiative and non-radiative rate constants analogous to fluid solution. *B* is a constant. The parameter, *p*, is the product of the observed second-order rate constant, k_2, and the initial concentration of ruthenium excited states, $[Ru^{2+*}]_{t=0}$. The details of this model have previously been described [45]. The second-order component arises from rapid *inter*-molecular energy transfer across the semiconductor surface that ultimately leads to triplet–triplet annihilation. This behavior is facilitated by high surface coverage and excitation irradiance. Monte-Carlo simulations have indicated an energy transfer rate constant of $(30\ \mathrm{ns})^{-1}$ at saturation surface coverage and second-order excited state decay was therefore expected for these long-lived Ru^{II*} rigid-rod sensitizers [45]. The abstracted first-order rate constants were similar but somewhat smaller than the corresponding values in fluid solution, Table 2.

3.4. *Transient absorption and charge injection studies*

Nanosecond transient absorption measurements were carried out in order to study the excited state behavior and quantify the charge injection processes. Solution data revealed a uniform decay over the whole spectral range studied, with clear isosbestic points and excited state lifetimes that agreed with those extracted from photoluminescence data, see Fig. 5 and supporting information. The transient absorption spectral data displayed the strong bleach of the ground state MLCT band usually expected for ^{3}MLCT states of $Ru(bpy)_3^{2+}$-type complexes. However, for $Ru(bpy)_3^{2+*}$ the excited state absorption at wavelengths greater than 550 nm is very small, while in all the rigid-rod excited states a very strong absorption in the red spectral region above 600 nm was observed. This band was attributed to enhanced triplet–triplet absorptions that result from the OPE-bridge. The relative intensity of the MLCT-bleach and the low energy excited state absorption is more or less the same for the *m*-Ru-Ipa-rod and the bimetallic compound (see Supporting Information), while it is significantly stronger in the resulting *p*-Ru-Ipa-rod spectrum. This fact can be rationalized in terms of the length of the bridge—the longer the OPE-bridge the stronger the low-lying absorption band.

Excited state behavior on nanocrystalline TiO_2 thin films immersed in either neat acetonitrile or in 0.1 M $LiClO_4$/acetonitrile was also examined by nanosecond transient absorption spectroscopy with 532 nm light excitation. In argon-purged acetonitrile solution, absorption changes monitored at the ground-excited state isosbestic points measured in fluid solution were measurably consistent with a small amount of the excited state injection without intentional addition of potential determining ions. With Li^+-containing acetonitrile solutions, less well-defined isosbestic points were observed but the amplitude of the absorption change

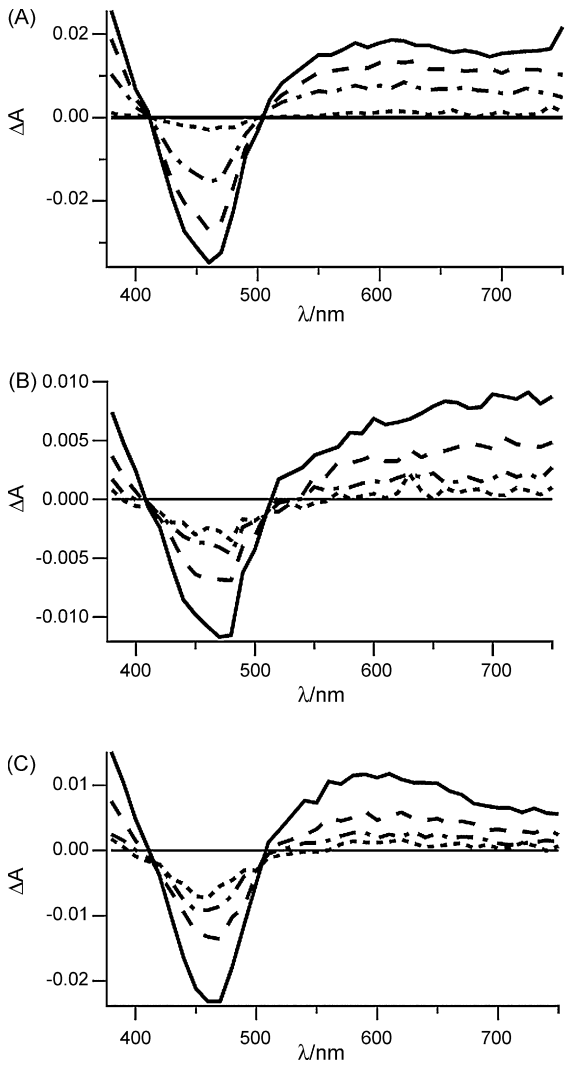

Fig. 5. Transient absorption spectra of *m*-Ru-Ipa-rod in (A) acetonitrile solution, (B) *m*-Ru-Ipa-rod/TiO_2 in neat acetonitrile, and (C) *m*-Ru-Ipa-rod/TiO_2 in 0.1 M $LiClO_4$ acetonitrile. Solid line = 100 ns, dashed line = 500 ns, dash-dot-dash line = 1500 ns and dotted line = 5000 ns.

was larger consistent with enhanced sub-nanosecond excited state injection. While solution data revealed uniform single exponential decay over the whole spectral range investigated, the contributions of both MLCT excited states and $Ru^{III}/TiO_2(e^-)$ interfacial charge separated states led to complicated kinetic behavior. The time scales were very different however, with negligible charge recombination of the interfacial charge-separated state over the first ~50 μs. Intervalence charge transfer between the two Ru-centers after excited state injection by the bi-metallic rod was considered, but no spectral evidence for such a process was observed.

Transient absorption comparative actinometry was used to quantify the excited state injection efficiency ~10 ns after pulsed laser excitation of the sensitized thin films in 0.3 M $LiClO_4$ acetonitrile solution. Measurements were made at a ground-excited state isosbestic point to minimize contributions from the MLCT excited state. The rods showed an excited state electron injection yield of $\phi_{inj} = 0.15 \pm 0.03$ for both isomers and the bimetallic rod. With the possible exception of *m*-Ru-Ipa-rod/TiO_2, the yields were considerably smaller than that inferred from the previously described excited state quenching studies with Li^+ cations. The poor agreement may be due to the very different excitation irradiances or to the presence of other static quenching processes induced by Li^+ cations. The $Ru^{III/II*}$ excited state reduction potentials were very similar for all the Ru-rigid rod sensitizers so there was no thermodynamic basis for a sensitizer dependent injection, Table 1. The theoretical calculations indicate that the optimized orientation has the isophthalic linker 45° with respect to the TiO_2 surface. This would place the *meta*-Ru^{II}-sensitizers on average closer to the semiconductor surface and may underlie their enhanced injection yields.

4. Conclusions

We have reported the photophysical and electrochemical properties of a series of Ru^{II}-rigid rods in solution and attached to TiO_2 nanocrystalline thin films. Whether the chromophore was conjugated with the bridge in the *meta*- or *para*-position had an influence on ground state light absorption properties with very small effects on the photoluminescent excited state. The excited state injection yields into nanocrystalline TiO_2 and the subsequent charge recombination rates were found to be insensitive to the isomer utilized. *Meta*-substitution enabled the synthesis of sensitizers with two Ru^{II}-sensitizers that displayed almost doubled sunlight absorption relative to the monomeric compound.

Theoretical calculations provided relevant information about the strength and stability of the different binding modes [26,27] and the optimized orientation of the Ru^{II}-rigid rod linkers relative to the TiO_2 surface [29]. First principles calculations suggested that the Ipa linker was bound more strongly to a model TiO_2 nanocrystal than a single carboxylic acid anchor group. The most stable binding mode involved the simultaneous attachment of both carboxylic acid anchor groups on the Ipa. The surface attachment chemistry causes the rigid rod sensitizers to tilt by approximately 45° relative to the surface normal. Although the details of the binding may be influenced by environmental effects, e.g. solvent–substrate interaction strengths, this supports the feasibility for using a single Ipa anchor group to firmly attach large linker-sensitizers or multichromophoric sensitizers to nanostructured metal oxide electrode materials such as TiO_2.

Acknowledgements

The Division of Chemical Sciences, Office of Basic Energy Sciences, Office of Energy Research, U.S. Department of Energy DE-FG02-96ER14662 (GJM) and DE-FG02-01ER15256 (EG) is gratefully acknowledged for research support. M.A. thanks the Swedish Research Council (Vetenskapsrådet) for a personal post-doctoral research grant (623-2007-2038). P.P. thanks the Swedish Research Council (Vetenskapsrådet) and the Swedish National Supercomputer Centre (NSC) for support.

Appendix A. Supplementary data

Supplementary data associated with this article can be found, in the online version, at doi:10.1016/j.jphotochem.2009.06.002.

References

[1] A. Hagfeldt, M. Gratzel, Molecular photovoltaics, Acc. Chem. Res. 33 (2000) 269–277.
[2] A. Juris, V. Balzani, F. Barigelletti, S. Campagna, P. Belser, A. Von Zelewsky, Ru(II) polypyridine complexes—photophysics, photochemistry, electrochemistry, and chemi-luminescence, Coord. Chem. Rev. 84 (1988) 85–277.
[3] L.C. Sun, L. Hammarstrom, B. Akermark, S. Styring, Towards artificial photosynthesis: ruthenium-manganese chemistry for energy production, Chem. Soc. Rev. 30 (2001) 36–49.
[4] F. Barigelletti, L. Flamigni, Photoactive molecular wires based on metal complexes, Chem. Soc. Rev. 29 (2000) 1–12.
[5] R. Ziessel, M. Hissler, A. El-Ghayoury, A. Harriman, Multifunctional transition metal complexes—information transfer at the molecular level, Coord. Chem. Rev. 178 (1998) 1251–1298.

[6] S. Ardo, G.J. Meyer, Photodriven heterogeneous charge transfer with transition-metal compounds anchored to TiO_2 semiconductor surfaces, Chem. Soc. Rev. 38 (2009) 115–164.
[7] K. Kalyanasundaram, M. Gratzel, Applications of functionalized transition metal complexes in photonic and optoelectronic devices, Coord. Chem. Rev. 177 (1998) 347–414.
[8] E. Galoppini, Linkers for anchoring sensitizers to semiconductor nanoparticles, Coord. Chem. Rev. 248 (2004) 1283–1297.
[9] E. Galoppini, W.Z. Guo, W. Zhang, P.G. Hoertz, P. Qu, G.J. Meyer, Long-range electron transfer across molecule-nanocrystalline semiconductor interfaces using tripodal sensitizers, J. Am. Chem. Soc. 124 (2002) 7801–7811.
[10] W.Z. Guo, E. Galoppini, G. Rydja, G. Pardi, Synthesis of a molecular tripod to anchor molecular coordination compounds to semiconductor nanoparticles, Tetrahedron Lett. 41 (2000) 7419–7421.
[11] D. Wang, R. Mendelsohn, E. Galoppini, P.G. Hoertz, R.A. Carlisle, G.J. Meyer, Excited state electron transfer from Ru(II) polypyridyl complexes anchored to nanocrystalline TiO_2 through rigid-rod linkers, J. Phys. Chem. B 108 (2004) 16642–16653.
[12] Q. Wei, E. Galoppini, Tripodal Ru(II) complexes with conjugated and non-conjugated rigid-rod bridges for semiconductor nanoparticles sensitization, Tetrahedron 60 (2004) 8497–8508.
[13] E. Galoppini, W.Z. Guo, P. Qu, G.J. Meyer, Long-distance electron transfer across molecule-nanocrystalline semiconductor interfaces, J. Am. Chem. Soc. 123 (2001) 4342–4343.
[14] P.G. Hoertz, R.A. Carlisle, G.J. Meyer, D. Wang, P. Piotrowiak, E. Galoppini, Organic rigid-rod linkers for coupling chromophores to metal oxide nanoparticles, Nano Lett. 3 (2003) 325–330.
[15] D. Wang, J.M. Schlegel, E. Galoppini, Synthesis of rigid-rod linkers to anchor chromophores to semiconductor nanoparticles, Tetrahedron 58 (2002) 6027–6032.
[16] J. Rochford, D. Chu, A. Hagfeldt, E. Galoppini, Tetrachelate porphyrin chromophores for metal oxide semiconductor sensitization: effect of the spacer length and anchoring group position, J. Am. Chem. Soc. 129 (2007) 4655–4665.
[17] O. Taratula, J. Rochford, P. Piotrowiak, E. Galoppini, R.A. Carlisle, G.J. Meyer, Pyrene-terminated phenylenethynylene rigid linkers anchored to metal oxide nanoparticles, J. Phys. Chem. B 110 (2006) 15734–15741.
[18] K. Kilså, E.I. Mayo, B.S. Brunschwig, H.B. Gray, N.S. Lewis, J.R. Winkler, Anchoring group and auxiliary ligand effects on the binding of ruthenium complexes to nanocrystalline TiO_2 photoelectrodes, J. Phys. Chem. B 108 (2004) 15640–15651.
[19] G.M. Hasselman, D.F. Watson, J.R. Stromberg, D.F. Bocian, D. Holten, J.S. Lindsey, G.J. Meyer, Theoretical solar-to-electrical energy-conversion efficiencies of perylene-porphyrin light-harvesting arrays, J. Phys. Chem. B 110 (2006) 25430–25440.
[20] P. Piotrowiak, E. Galoppini, Q. Wei, G.J. Meyer, R. Wiewior, Subpicosecond photoinduced charge injection from "Molecular tripods" into mesoporous TiO_2 over the distance of 24 angstroms, J. Am. Chem. Soc. 125 (2003) 5278–5279.
[21] K.R.J. Thomas, A.L. Thompson, A.V. Sivakumar, C.J. Bardeen, S. Thayumanavan, Energy and electron transfer in bifunctional non-conjugated dendrimers, J. Am. Chem. Soc. 127 (2005) 373–383.
[22] A.L. Thompson, K.M. Gaab, J.J. Xu, C.J. Bardeen, T.J. Martinez, Variable electronic coupling in phenylacetylene dendrimers: the role of forster, dexter, and charge-transfer interactions, J. Phys. Chem. A 108 (2004) 671–682.
[23] A.L. Thompson, T.S. Ahn, K.R.J. Thomas, S. Thayumanavan, T.J. Martinez, C.J. Bardeen, Using meta conjugation to enhance charge separation versus charge recombination in phenylacetylene donor-bridge-acceptor complexes, J. Am. Chem. Soc. 127 (2005) 16348–16349.
[24] P. Persson, R. Bergstrom, L. Ojamae, S. Lunell, Quantum-chemical studies of metal oxides for photoelectrochemical applications, Adv. Quantum Chem. 41 (2002) 203–263.
[25] W.R. Duncan, O.V. Prezhdo, Theoretical studies of photoinduced electron transfer in dye-sensitized TiO_2, Annu. Rev. Phys. Chem. 58 (2007) 143–184.
[26] P. Persson, M.J. Lundqvist, Calculated structural and electronic interactions of the ruthenium dye N3 with a titanium dioxide nanocrystal, J. Phys. Chem. B 109 (2005) 11918–11924.
[27] P. Persson, A. Stashans, R. Bergstrom, S. Lunell, Periodic INDO calculations of organic adsorbates on a TiO_2 surface, Int. J. Quant. Chem. 70 (1998) 1055–1066.
[28] P. Persson, M.J. Lundqvist, R. Ernstorfer, W.A. Goddard, F. Willig, Quantum chemical calculations of the influence of anchor-cum-spacer groups on femtosecond electron transfer times in dye-sensitized semiconductor nanocrystals, J. Chem. Theory Comput. 2 (2006) 441–451.
[29] M.J. Lundqvist, E. Galoppini, G.J. Meyer, P. Persson, Calculated optoelectronic properties of ruthenium tris-bipyridine dyes containing oligophenyleneethynylene rigid rod linkers in different chemical environments, J. Phys. Chem. A 111 (2007) 1487–1497.
[30] M. Sprecher, R. Breslow, O. Uziel, T.M. Link, Monosubstituted 2,2′-bipyridines, Org. Prep. Proc. Int. 26 (1994) 696–701.
[31] K. Araki, T. Mutai, Y. Shigemitsu, M. Yamada, T. Nakajima, S. Kuroda, I. Shimao, 6-amino-2,2′-bipyridine as a new fluorescent organic compound, J. Chem. Soc., Perkin Trans. 2 (1996) 613–617.
[32] R. Argazzi, C.A. Bignozzi, T.A. Heimer, F.N. Castellano, G.J. Meyer, Enhanced spectral sensitivity from ruthenium(II) poplypyridyl based photovoltaic devices, Inorg. Chem. 33 (1994) 5741–5749.
[33] B.V. Bergeron, G.J. Meyer, Reductive electron transfer quenching of MLCT excited states bound to nanostructured metal oxide thin films, J. Phys. Chem. B 107 (2003) 245–254.
[34] M.J. Lundqvist, M. Nilsing, P. Persson, S. Lunell, DFT study of bare and dye-sensitized TiO2 clusters and nanocrystals, Int. J. Quant. Chem. 106 (2006) 3214–3234.
[35] P. Persson, R. Bergstrom, S. Lunell, Quantum chemical study of photoinjection processes in dye-sensitized TiO_2 nanoparticles, J. Phys. Chem. B 104 (2000) 10348–10351.
[36] M.J. Lundqvist, M. Nilsing, S. Lunell, B. Akermark, P. Persson, Spacer and anchor effects on the electronic coupling in ruthenium-bis-terpyridine dye-sensitized TiO_2 nanocrystals studied by DFT, J. Phys. Chem. B 110 (2006) 20513–20525.
[37] A.D. Becke, Density-functional thermochemistry. 3. The role of exact exchange, J. Chem. Phys. 98 (1993) 5648–5652.
[38] P. Persson, L. Ojamae, Periodic Hartree-Fock study of the adsorption of formic acid on ZnO(1 0 1 0), Chem. Phys. Lett. 321 (2000) 302–308.
[39] Gaussian 03 Revision C.02 G.W.T. M.J. Frisch, H.B. Schlegel, G.E. Scuseria, M.A. Robb, J.R. Cheeseman, J.A. Montgomery, Jr., T. Vreven, K.N. Kudin, J.C. Burant, J.M. Millam, S.S. Iyengar, J. Tomasi, V. Barone, B. Mennucci, M. Cossi, G. Scalmani, N. Rega, G.A. Petersson, H. Nakatsuji, M. Hada, M. Ehara, K. Toyota, R. Fukuda, J. Hasegawa, M. Ishida, T. Nakajima, Y. Honda, O. Kitao, H. Nakai, M. Klene, X. Li, J.E. Knox, H.P. Hratchian, J.B. Cross, V. Bakken, C. Adamo, J. Jaramillo, R. Gomperts, R.E. Stratmann, O. Yazyev, A.J. Austin, R. Cammi, C. Pomelli, J.W. Ochterski, P.Y. Ayala, K. Morokuma, G.A. Voth, P. Salvador, J.J. Dannenberg, V.G. Zakrzewski, S. Dapprich, A.D. Daniels, M.C. Strain, O. Farkas, D.K. Malick, A.D. Rabuck, K. Raghavachari, J.B. Foresman, J.V. Ortiz, Q. Cui, A.G. Baboul, S. Clifford, J. Cioslowski, B.B. Stefanov, G. Liu, A. Liashenko, P. Piskorz, I. Komaromi, R.L. Martin, D.J. Fox, T. Keith, M.A. Al-Laham, C.Y. Peng, A. Nanayakkara, M. Challacombe, P. M.W. Gill, B. Johnson, W. Chen, M.W. Wong, C. Gonzalez, J.A. Pople, Gaussian, Inc., Wallingford CT, 2004.
[40] P.K. Sudeep, P.V. James, K.G. Thomas, P.V. Kamat, Singlet and triplet excited-state interactions and photochemical reactivity of phenyleneethynylene oligomers, J. Phys. Chem. A 110 (2006) 5642–5649.
[41] A. Staniszewski, S. Ardo, Y. Sun, F.N. Castellano, G.J. Meyer, Slow cation transfer follows sensitizer regeneration at anatase TiO_2 interfaces, J. Am. Chem. Soc. 130 (2008) 11586–11587.
[42] C.A. Kelly, F. Farzad, D.W. Thompson, J.M. Stipkala, G.J. Meyer, Cation-controlled interfacial charge injection in sensitized nanocrystalline TiO_2, Langmuir 15 (1999) 7047–7054.
[43] D.P. Rillema, C.B. Blanton, R.J. Shaver, D.C. Jackman, M. Boldaji, S. Bundy, L.A. Worl, T.J. Meyer, MLCT-dd energy-gap in pyridyl pyrimidine and bis(pyridine) complexes of ruthenium(II), Inorg. Chem. 31 (1992) 1600–1606.
[44] J.V. Caspar, T.J. Meyer, Photochemistry of MLCT excited-states—effect of nonchromophoric ligand variations on photophysical properties in the series cis-Ru(bpy)2(L)22+, Inorg. Chem. 22 (1983) 2444–2453.
[45] C.A. Kelly, F. Farzad, D.W. Thompson, G.J. Meyer, Excited-state deactivation of ruthenium(II) polypyridyl chromophores bound to nanocrystalline TiO_2 mesoporous thin films, Langmuir 15 (1999) 731–737.